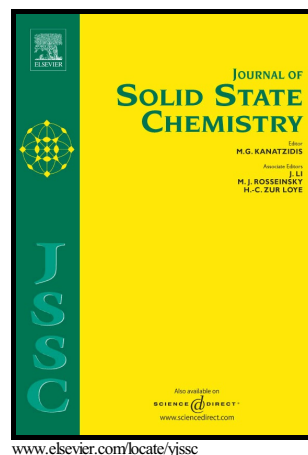


Author's Accepted Manuscript

Self-assembly of novel manganese (II) compounds based on bifunctional-group ligands: synthesis, structures, and magnetic properties

Juan-zhi Yan, Li-ping Lu, Miao-li Zhu, Si-si Feng



PII: S0022-4596(18)30124-5
DOI: <https://doi.org/10.1016/j.jssc.2018.03.035>
Reference: YJSSC20161

To appear in: *Journal of Solid State Chemistry*

Received date: 31 January 2018
Revised date: 19 March 2018
Accepted date: 29 March 2018

Cite this article as: Juan-zhi Yan, Li-ping Lu, Miao-li Zhu and Si-si Feng, Self-assembly of novel manganese (II) compounds based on bifunctional-group ligands: synthesis, structures, and magnetic properties, *Journal of Solid State Chemistry*, <https://doi.org/10.1016/j.jssc.2018.03.035>

This is a PDF file of an unedited manuscript that has been accepted for publication. As a service to our customers we are providing this early version of the manuscript. The manuscript will undergo copyediting, typesetting, and review of the resulting galley proof before it is published in its final citable form. Please note that during the production process errors may be discovered which could affect the content, and all legal disclaimers that apply to the journal pertain.

Self-assembly of novel manganese (II) compounds based on bifunctional-group ligands: synthesis, structures, and magnetic properties

Juan-zhi Yan^{a,b}, Li-ping Lu^a, Miao-li Zhu^{a,c*}, Si-si Feng^{a,c*}

^aInstitute of Molecular Science, Key Laboratory of Chemical Biology and Molecular Engineering of the Education Ministry, Shanxi University, Taiyuan, Shanxi, 030006, PR China.

^bTaiyuan University, Taiyuan, Shanxi, 030032, PR China.

^cKey Laboratory of Materials for Energy Conversion and Storage of Shanxi Province; Shanxi University, Taiyuan, Shanxi, 030006, PR China.

miaoli@sxu.edu.cn

ssfeng@sxu.edu.cn

***Corresponding authors.** Tel: ++86-351-7017974; Fax: ++86-351-7011022.

Abstract

Four manganese (II) compounds are obtained by the reaction of manganese salts, triazole-derivatives and auxiliary reagents in aqueous solution or mix-solvents by routine or hydrothermal reactions. X-ray crystal structure analyses reveal that a

neutral 0D compound $[\text{Mn}(\text{Hmctrz})_2(\text{H}_2\text{O})_2]$ (**1**) ($\text{H}_2\text{mctrz} = 1H\text{-}1,2,4\text{-triazole-}3\text{-carboxylic acid}$) displays a centro-symmetric mononuclear octahedral entity with two Hmctrz^- anions and two water molecules; two neutral 2D clusters $[\text{Mn}(\text{Hdctrz})(\text{H}_2\text{O})_2]_n$ (**2**) ($\text{H}_3\text{dctrz} = 1H\text{-}1,2,4\text{-triazole-}3,5\text{-dicarboxylic acid}$) and $[\text{Mn}_2(\text{pbtrz})(\text{btca})]_n \cdot 4n\text{H}_2\text{O}$ (**3**) ($\text{pbtrz} = 1,3\text{-bis}(1,2,4\text{-triazol-}1\text{-yl})\text{-propane}$ & $\text{H}_4\text{btca} = \text{benzene-}1,2,4,5\text{-tetracarboxylic acid}$) possess layer structures with Hdctrz^{2-} linkers (**2**) and $\text{Mn(II)-pbtrz-Mn(II)}$ building blocks periodically extended by $\mu\text{-btca}^{4-}$ connectors (**3**); $[\text{Mn}(\text{pbtrz})]_n \cdot n\text{OAc} \cdot n\text{OH}$ (**4**) shows a 3D diamond-shaped cationic framework with the anion void volume of 49.2%. Nitrogenous bases are used as the auxiliary ligand in compound **3** and the temple ligand in compounds **1**, **2**, and **4**. Compounds **1–4** show antiferromagnetic coupling that has been fitted by different models with the molecular field approximate with $D = -0.129(1) \text{ cm}^{-1}$ for **1**, $J = -0.354(4) \text{ cm}^{-1}$ for **2** and $J = -0.696(6) \text{ cm}^{-1}$ for **3**, respectively. The magnetic differences can be related to different superexchange interactions transmitted by the crystal lattice and/or the zero field splitting (ZFS) of the ${}^6\text{A}_{1g}$ single-ion states of **1** and the *syn-anti*- COO^- of **2** as well as the mixed magnetic bridges of $\mu_1\text{-O}$ and $\mu\text{-pbtrz-}\mu\text{-COO}^-$ of **3**.

Keywords

1,2,4-triazole; Mn(II) compounds; structures; magnetism.

1. Introduction

Over the last decade, extensive researches have been carried out for the structures and magnetic properties of coordination polymers [1–4]. Manganese compounds have been especially investigated because the high spin ground states may be obtained from the strong exchange interactions between the 3d electrons [5, 6]. Consequently, manganese compounds show different types of magnetic behaviour such as ferromagnetic [7, 8], antiferromagnetic [9–11], metamagnetic [12], spin-canting [13] and etc. Besides the spin carrier, the judicious choice of bridging groups is also crucial to the design of molecular magnets. As is well-known, the carboxylate group not only transfers moderate or strong ferromagnetic or antiferromagnetic magnetic interaction, but also constructs various interesting architectures with rich coordination modes such as chelating, terminal and bridging *syn-syn*, *anti-anti*, or *syn-anti* [14, 15]. Meanwhile, 1,2,4-triazolyl groups as nitrogen-based donors have been strongly recognized as the main factors for efficient magnetic super-exchange between the nearest spin carriers [16] due to varied coordination characteristics [17–21], the asymmetric tridentate bridging mode [22] as well as the well-suited distance [23–27]. Furthermore, the exocyclic substitutes of the 1,2,4-triazolate derivatives with end-on coordination capacity, such as carboxylate-, mono- and/or di-amino, can also synergistically assist the structural diversity [28] and magnetic interactions either by coordination with spin carriers or by weak non-covalent interactions [19, 21, 29–31]. Up to now, most manganese complexes based on triazolate-carboxylate are reported with either ferromagnetic or antiferromagnetic interactions [32–34]. However, it is

2. Experimental

All chemicals were of standard commercial grade and were used directly without further purification. The ligand H₃dctrz was prepared and purified according to the literature [36]. IR spectra data were recorded on a BRUKER TENSOR27 spectrometer with KBr disks. Elemental analyses for C, H and N were performed on a CHN-O-Rapid instrument. Powder X-ray diffraction (PXRD) patterns were collected on a Bruker D8 Advance X-ray diffractometer using Cu-K α radiation ($\lambda = 1.540598 \text{ \AA}$) at 30 kV and 15 mA. The simulated patterns of **1–4** were derived from free Mercury Version 2.2 software. Thermogravimetric (TG) studies were carried out on a Dupont thermal analyzer with temperature range 298–1073 K under N₂ flow with a heating rate of 20 K min⁻¹. Variable temperature (1.8–300 K) magnetic susceptibilities of crystalline samples of the complexes were measured on a Quantum Design MPMS SQUID magnetometer with an applied field of 1000 Oe.

2.1. Synthesis of [Mn(Hmctrz)₂(H₂O)₂] (1)

MnCl₂·4H₂O (0.198 g, 1.0 mmol) in 3.0 mL of aqueous solution was slowly added into a flask containing H₃dctrz (0.078 g, 0.5 mmol) and pbtrz (0.08 g, 0.5 mmol) in 10.0 mL of aqueous solution. The reacting solution was kept stirring for 6.0 h. The precipitate was filtrated, and colourless crystals were isolated from the filtrate within 6 weeks. Yield: 0.164 g (52.2% based on Mn(II)). Elemental analysis (EA) for calcd. **1** (C₆H₈N₆O₆Mn, 315.12): C 16.96, H 1.78, N 22.25; found: C 17.34, H 1.94, N 21.22%. IR (cm⁻¹, s = strong, m = medium, w = weak): 3361s, 3122s, 1625s, 1476s, 1411s, 1368w, 1353w, 1296s, 1162w, 1012m, 984w, 892w, 841m, 670m.

2.2. Synthesis of $[Mn(Hdctrz)(H_2O)_2]_n$ (2)

NaHCO₃ (0.042 g, 0.5 mmol) in 5.0 mL of aqueous solution was added into a flask containing aqueous solution of H₃dctrz (0.078 g, 0.5 mmol) with stirring, MnCl₂·4H₂O (0.198 g, 1.0 mmol) powder was directly added, and then a 4.0 mL of phen (0.10 g, 0.5 mmol) ethanol solution was added dropwise. The resulting solution was kept stirring for 6.0 h. The precipitate was filtrated, and colourless crystals were isolated from the filtrate within 4 weeks. Yield: 0.114 g (46.4% based on Mn(II)). EA calcd. for **2** (C₄H₅N₃O₆Mn, 246.05): C 19.53, H 2.05, N 17.08. Found: C 19.72, H 2.59, N 16.87%. IR (cm⁻¹): 3221s, 3101s, 1619s, 1517m, 1496m, 1454m, 1404s, 1356w, 1300s, 1162w, 1056s, 905w, 828m, 813w, 729m, 661m, 600w.

2.3. Synthesis of $[Mn_2(pbtrz)(btca)]_n \cdot 4nH_2O$ (3)

A 5.0 mL methanol solution of MnCl₂·4H₂O (0.396 g, 2.0 mmol) was added into a 10.0 mL aqueous solution of pbtrz (0.179 g, 1.0 mmol) in a flask with stirring and then a 5.0 mL aqueous solution of H₄btca (0.051 g, 0.2 mmol) and N(C₂H₅)₃ (50.0 μL) was dropped to the above mixture. After 4h, the resulting solution was filtrated, and colorless crystals were isolated from the filtrate within 4 weeks. Yield: 0.290 g (43.7% based on Mn(II)). EA calcd. for **3** (C₁₇H₂₆N₆O₁₅Mn₂, 664.32): C 30.74, H 3.94, N 12.65. Found: C 31.25, H 4.07, N 11.57%. IR (cm⁻¹): 3400s, 3200m, 3108m, 2295w, 1625s, 1420m, 1384s, 1340s, 1131m, 981w, 809m, 668m, 538m.

2.4. Synthesis of $[Mn(pbtrz)]_n \cdot nOAc \cdot nOH$ (4)

A mixture of pbtrz (0.090 g, 0.5 mmol), C₆H₄(NH₂)(SO₃H) (0.017 g, 0.1 mmol), Mn(OAc)₂·4H₂O (0.245 g, 1.0 mmol), KOH (2.0%, 30 uL), CH₃OH (8.0 mL) and

DMF (1.0 mL) was sealed in a 25.0 mL Teflon-lined stainless steel autoclave and heated at 383 K for 3 days, and then slowly cooled to room temperature. Colourless crystals of **4** were obtained, and the yield was 0.174 g (56.3% based on Mn(II)). EA calcd. for **4** (C₉H₁₄N₆O₃Mn, 309.20): C 34.96, H 4.56, N 27.18. Found: C 35.12, H 4.09, N 26.87%. IR (cm⁻¹): 3433m, 3108s, 1670s, 1524s, 1384s, 1280m, 1218w, 1139s, 1103w, 1043w, 981w, 885w, 668m.

2.5. X-ray crystallography

Single-crystal X-ray diffraction data for compounds **1**, **4** were collected in Beijing Synchrotron Radiation Facility (BSRF) beamline 3W1A which mounted with a MARCCD-165 detector ($\lambda = 0.72000 \text{ \AA}$) with storage ring working at 2.5 GeV. In the process, the crystal was protected by liquid nitrogen at 100(2) K. Data were collected by the program Marccd and processed using HKL 2000 [37]. The data of the compounds **2**, **3** were collected on a Bruker Smart Apex II with CCD area detector diffractometer Mo-K α ($\lambda = 0.71073 \text{ \AA}$) at room temperature. Cell parameters were determined using SMART software [38]. Data reduction and corrections were performed using SAINTPlus. Absorption corrections were applied by using the multi-scan program SADABS [38]. All the structures were solved by the direct methods and refined by the full-matrix least-squares technique using the SHELXS-2014 [38]. All non-hydrogen atoms were refined anisotropically. The hydrogen atoms except those of water molecules were generated geometrically and refined isotropically using the riding model. Due to the highly disordered OH⁻ and CH₃COO⁻ in **4**, their contribution to densities was modelled using the SQUEEZE

routine in PLATON [39]. The crystallographic data for the four compounds are listed in Table 1, and the selected bond lengths and angles are shown in Tables S1 and hydrogen bonding data are given in Table S2.

Table 1. Crystal data and structure refinement parameters for compounds 1–4

Compounds	1	2	3	4
CCDC	1060382	1060383	1060384	1060385
Formula	C ₆ H ₈ N ₆ O ₆ Mn	C ₄ H ₅ N ₃ O ₆ Mn	C ₁₇ H ₂₆ N ₆ O ₁₅ Mn ₂	C ₂₇ H ₄₂ N ₁₈ O ₉ Mn ₃
F_w	315.12	246.05	664.32	927.60
T/K	100(2)	298(2)	296(2)	100(2)
Wavelength/Å	0.72000	0.71073	0.71073	0.72000
Crystal system	Monoclinic	Monoclinic	Triclinic	Cubic
Space group	$P2_1/c$	$P2_1/c$	$P\bar{1}$	$Im\bar{3}d$
$a/\text{Å}$	9.177(2)	7.160(1)	9.696(2)	26.600(3)
$b/\text{Å}$	8.775(2)	10.212(1)	11.612(1)	26.600(3)
$c/\text{Å}$	6.855(1)	10.518(1)	11.637(1)	26.600(3)
$\alpha/^\circ$	90	90	85.406(1)	90
$\beta/^\circ$	93.13(3)	95.256(1)	89.370(1)	90
$\gamma/^\circ$	90	90	75.167(1)	90
$V/\text{Å}^3$	551.2(1)	765.7(1)	1262.37(5)	18821(6)
Z	2	4	2	16
$D_c/\text{g}\cdot\text{cm}^{-3}$	1.899	2.134	1.748	1.309
μ/mm^{-1}	1.236	1.736	1.086	0.879
$F(000)$	318	492	680	7632
R_{int}	0.0315	0.0363	0.038	0.0533
$R_1/wR_2(I > 2\sigma(I))^a$	0.0372/0.1308	0.0242/0.0590	0.0420/0.0943	0.1022/0.3079
$R_1/wR_2(\text{all data})^b$	0.0427/0.1466	0.0306/0.0620	0.0714/0.1047	0.1109/0.3246
GOF on F^2	1.041	1.074	1.002	1.520
$\rho_{\text{max, min.}}/\text{e}\text{Å}^{-3}$	0.569, -0.655	0.247, -0.253	0.899, -0.732	0.941, -0.663

$$^a R_1 = \sum \left(|F_o| - |F_c| \right) / \sum |F_o| \quad ^b wR_2 = \left[\sum w(F_o^2 - F_c^2)^2 / \sum w(F_o^2)^2 \right]^{1/2}$$

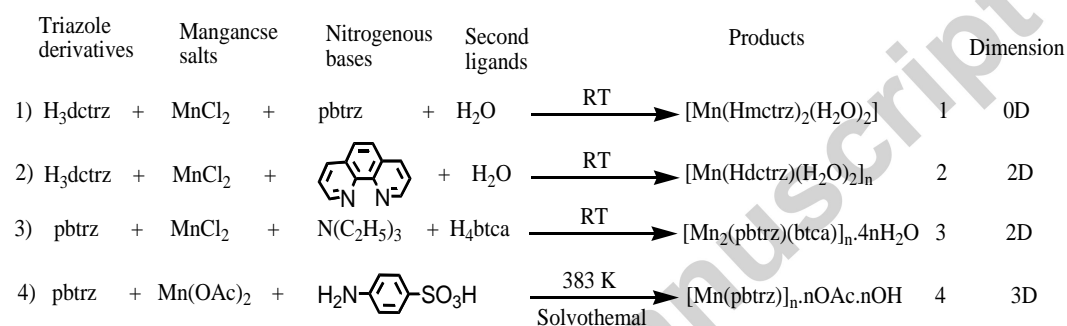
3 Results and discussion

3.1. Synthesis

H₃dctrz is a simple planar hepta-dentate ligand with a delocalized multi- π -electron backbone [30]. The ligand can not only be partially or fully deprotonated (H₂dctrz⁻, Hdctrz²⁻, & dctrz³⁻) under different pH values, but also decompose and lose one or two carboxylates in synthesis reactions. In our previous work [30], we proposed a pattern designator (M_{hijk}^{nlm}) to specify the rich coordination modes of H₃dctrz, where sign M for the number of coordinated metal atoms, nlm and $hijk$ for the position and the number of donors coordinated N and O atoms. The ligand H₂mctrz in **1** is a decarboxylate of H₃dctrz, which loses one carboxylate to ingenious structures [6, 40, 41]. In compound **2**, H₃dctrz is partially deprotonated to form Hdctrz²⁻, and we find a new coordinated mode: 3_{1110}^{001} , which is different from reported complexes [Mn₃(dctrz)₂(H₂O)₈]_n (3_{2001}^{110}) [30] and [Mn(Hdctrz)(H₂O)₃]_n (2_{0110}^{001}) [42]. Compared with H₃dctrz, pbtrz is a flexible double triazole ligand, in which four potential coordination sites can connect the metal cations to high-dimensional frameworks and -CH₂ groups can provide different conformations such as *anti-anti*, *anti-gauche*, and *gauche-gauche* [43–45]. Both ligands can bridge metal cations through 1,2,4-triazole or carboxylate groups to form diversity structures [33]. The second ligands such as nitrogen-based one can result in the spatial extension to build more complicated structures, and further change intra- and inter- magnetic interactions of the complexes. Moreover, they can also act as the templates to bring out H₄btca to employ eight oxygen donors from carboxylate group to spread the structural unit and to form a 2D

coordination polymer. However, in compounds **1**, **2** and **4** nitrogen-based ligands act as the templates, without of which, the compounds cannot be obtained under the same conditions. Compounds **1–3** are synthesized under ambient condition while **4** is formed under the solvothermal reaction with mild temperature (383 K), indicating that high temperature is favourable to form this structure.

Scheme 2. Synthesis routes of **1–4**



3.2. FT-IR spectra

The IR spectra of these compounds display the characteristic bands of the hydroxyl, triazole and carboxylate groups. Compounds **1–4** show strong broad bands around 3361, 3221, 3400 and 3442 cm⁻¹, respectively, suggesting the presence of O–H and N–H groups (Fig. S1). The strong absorption peaks, 1476 cm⁻¹ (**1**), 1496 cm⁻¹ (**2**), 1427 cm⁻¹ (**3**) and 1524 cm⁻¹ (**4**), are attributed to the C=N stretching vibration of the triazole ring. In fact, the IR absorption of carboxylate group is very complicated due to its coordination diversity with metal cations. The characteristic bands of the carboxylate groups in **1–3** appear in the usual region. The characteristic multiple bands for the asymmetric (ν_{as}) and symmetric (ν_{s}) stretching vibrations of the

carboxylate groups are observed between 1600 and 1400 cm^{-1} , and their different separations ($\Delta\nu = \nu_{\text{as}} - \nu_{\text{s}}$) suggest the presence of the mono-dentate, bi-dentate chelating and bridging modes of the carboxylate groups [46]. Interestingly, in compound **4**, strong bands occurring at approximately 1670 cm^{-1} and 1384 cm^{-1} suggest that the CH_3COO^- anion is not involved in the coordination, which is in good agreement with its structure from single crystal X-ray diffraction data.

3.3 Structure description

Crystal Structure of $[\text{Mn}(\text{Hmctrz})_2(\text{H}_2\text{O})_2]$ (**1**). H_2mctrz is not in the initial recipes (Scheme 2). It is formed by the decarboxylation reaction of H_3dctrz under acidic conditions. Compound **1** crystallizes in the monoclinic $P2_1/c$ space group with centrosymmetric mononuclear molecule (Fig. 1a). It is assembled into a 3D supramolecular network by abundant hydrogen-bonding interactions (Fig. 1b). The asymmetrical unit of **1** contains one crystallographic independent Mn(II) cation, one deprotonated Hmctrz^- and one terminal coordinated water molecule. Each Mn(II) cation, locating on the inversion center, has octahedral coordination geometry (MnN_2O_4) from two nitrogen (N1 & N1^i) and two oxygen (O1 & O1^i) of two symmetry-related Hmctrz^- ligands in the equatorial plane and two oxygen (O3 & O3^i) of two water molecules in the axial sites. All the bond distances and angles fall in the normal range [18, 24, 47, 48]. The axial distance of Mn–O (2.190(2) Å) is slightly longer than that of isostructural compound $[\text{Zn}(\text{Hmctrz})_2(\text{H}_2\text{O})_2]$ (2.133(1) Å), and shorter than that of $[\text{Cu}(\text{Hmctrz})_2(\text{H}_2\text{O})_2]$ (2.400(3) Å) [49] which is due to

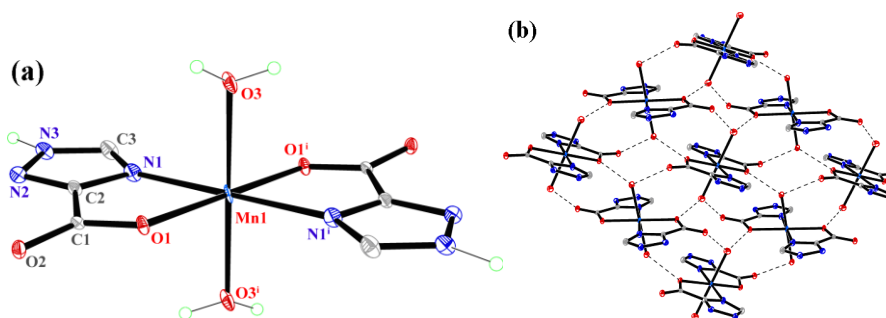


Fig. 1. (a) Coordination environment of Mn(II) in **1** with 30% thermal ellipsoids, symmetry code:

$i\ 1-x, -y + 2, -z$. (b) 2D supra-molecular layer structure *via* H-bonds of **1** (Cyan: Mn; Red: O;

Grey: C; Blue: N)

Jahn-Teller effect of Cu(II) cation.

As shown in Fig. 1b and Table S2, there are strong O–H···O hydrogen bonds [50] (2.729(3) Å, 2.714(3) Å) between carboxylate oxygen and coordinated water molecules. These O–H···O interactions assemble the basic $[\text{Mn}(\text{Hmctrz})_2(\text{H}_2\text{O})_2]$ unit into 2D layer structures paralleling to the crystallographic *ac* plane. The neighboring 2D layers stack in ABAB mode (Fig. 1b). The N–H···O interactions with a distance of 2.717(4) Å between neighboring layers build 2D structures into a 3D supramolecular architecture. The strong hydrogen bonds might prevent nitrogen atoms of 1- and 2-positional triazole from coordinating to Mn(II) even though nitrogen atoms are strong donors [49].

Crystal Structure of $[\text{Mn}(\text{Hdctrz})(\text{H}_2\text{O})_2]_n$ (**2**). Compound **2** crystallizes in the monoclinic $P2_1/c$ space group and displays a 2D network sheet which is constructed by Mn(II)-Hdctrz²⁻ layers, exhibiting a 2D 3-connected symbolized as 6^3 topological

structure. There is one crystallographic independent Mn(II) cation, one deprotonated Hdctrz²⁻ anion and two coordinated water molecules in the asymmetrical unit.

As shown in Fig. 2a, Mn(II) cation in **2** is surrounded by one nitrogen (N1) and three oxygen (O1, O2ⁱ & O3ⁱⁱ) from two individual Hdctrz²⁻ anions and two coordination water molecules (O5 & O6), forming a distorted octahedral coordination arrangement (MnNO₅), in which the Mn–O distances of 2.124(1)–2.244(1) Å are slightly shorter than that of Mn–N separations (2.260(1) Å).

Each ligand Hdctrz²⁻ connects three Mn(II) cations to construct a tetranuclear cluster [Mn₄(Hdctrz)₄] in two different bridging fashions: the one *syn-anti-μ₂-η¹:η¹*

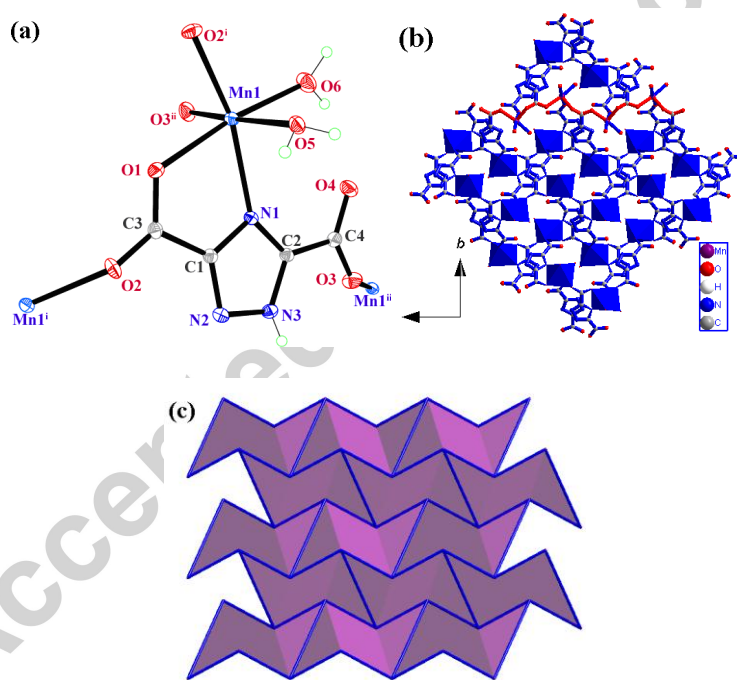


Fig. 2. (a) Coordination environment of Mn(II) in **2** with 30% thermal ellipsoids, symmetry codes: i $x, -y + 5/2, z + 1/2$; ii $-x + 1, y + 1/2, -z + 3/2$. (b) View of 2D polyhedrons of MnNO₅ and network sheets (the red line shows the Mn–OCO–Mn chain). (c) 2D 3-c (6^3) topologic network.

carboxylate with Mn1⋯Mn1ⁱ distances of 5.955(1) Å, and the other μ_2 -N1, O3-Hdctrz²⁻ through(–N–C–C–O–) connection with Mn1⋯Mn1ⁱⁱ distances of

7.069(1) Å (Fig. 2a and relative symmetry codes). Then, $[\text{Mn}_4(\text{Hdctrz})_4]$ unit joins each other *via* the Hdctrz^{2-} to build 2D network sheets paralleling to the crystallographic *bc* plane (Fig. 2b). Furthermore, together with the carboxylate O and triazole N atoms, two coordinated water molecules reinforce the network by hydrogen bonds to carboxylate oxygen. Taking Mn(II) cations as 3-connected nodes and two parallel Hdctrz^{2-} ($\text{Mn}\cdots\text{Mn}$, 9.618(2) Å) and COO^- ($\text{Mn}\cdots\text{Mn}$, 5.955(1) Å) as linkers, the 2D polymeric layer can be simplified to a 3-connected symbolized as (6^3) topologic network (Fig. 2c).

Crystal Structure of $[\text{Mn}_2(\text{pbtrz})(\text{btca})]_n \cdot 4\text{nH}_2\text{O}$ (**3**). X-ray diffraction analysis indicates that compound **3** also forms a 2D network sheet in which μ_2 -pbtrz ligand coordinate with Mn(II) forming subunits periodically, then they are extended by μ_6 -btca⁴⁻ connectors. The asymmetric unit of **3** contains two crystallographic independent Mn(II) cations, one neutral pbtrz ligand, two half deprotonated btca⁴⁻ anions, three coordinated water molecules and four disordered lattice water molecules.

As shown in Fig. 3a, both Mn(II) cations adopt distorted octahedral geometries with MnNO_5 donor sets. The Mn1 octahedron is well defined by one triazolyl nitrogen (N1), two carboxylate oxygen (O3 & O8) from the different btca⁴⁻ anions and three oxygen atoms (O9, O10 & O11) from coordinated water molecules. The Mn2 cation is coordinated by one triazolyl nitrogen (N6ⁱⁱ), four carboxylate oxygen atoms (O1, O2, O7 & O2ⁱ) from two different btca⁴⁻ anions and one sharing oxygen atom O9 from coordinated water. The bond lengths of Mn–N and Mn–O are comparable to

other Mn(II) complexes mixed pbtrz and carboxylate ligands [1,3,22]. Each pair of MnNO₅ octahedron forms a dimer *via* corner-sharing, in which both Mn(II) cations are bridged by one $\mu_{1,1}$ -O9 water molecule and two $\mu_{1,3}$ -OCO carboxylates group. That is, two carboxylate groups with the μ_2 - $\eta^1:\eta^1$ -OCO chelating fashion, together with one $\mu_{1,1}$ -O9 atom serving as two Mn(II) cations, and Mn1–O9–Mn2 angle is 109.03(1)°. The neighbor Mn(II) cations with the Mn2[⋯]Mn2ⁱ distance of 5.646(1) Å. Thus, two dimers are linked by two pbtrz and two neighbor carboxylates (in the μ_1 - $\eta^1:\eta^0$ coordination mode) from btca⁴⁻ forming the Mn₂btca-COOⁿ⁻ (Mn₂N₂O₇) closed loops (SBU-1) with the Mn1[⋯]Mn2 distance of 3.708(1) Å, and the ligands together with four Mn(II) cations in the tetramer cage have a parallelogram conformation with the Mn2[⋯]Mn2ⁱⁱ distance of 5.711(1) and Mn1[⋯]Mn2ⁱⁱ 7.338(3) Å. Further these cages make up of a layered organic-inorganic sheet *via* meta- and para-carboxylates in directions of *a* and *b* axis respectively to form 2D chair modes (Fig. 3b).

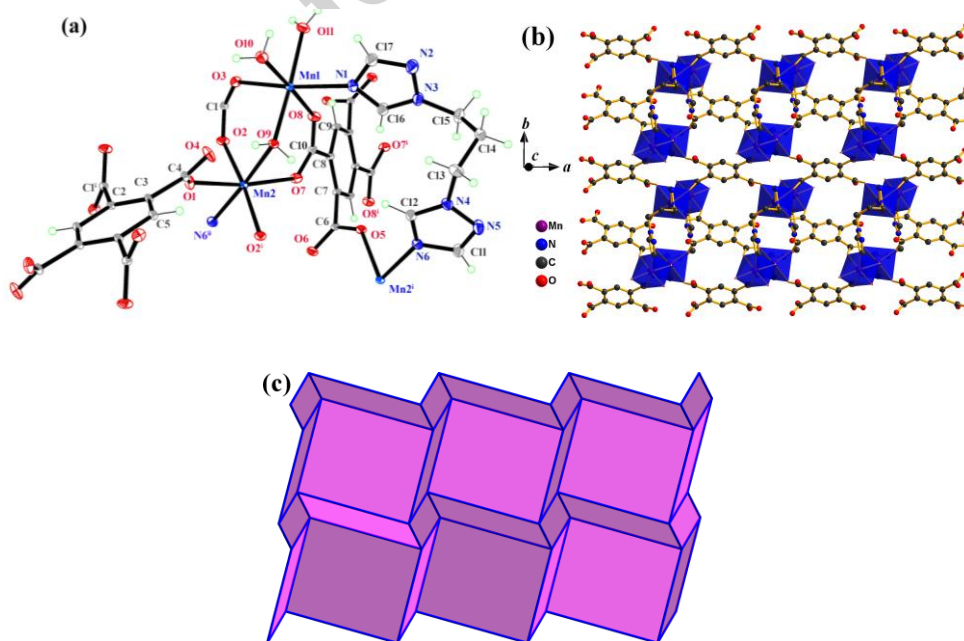


Fig. 3. (a) Coordination environments of Mn(II) in **3** with 30% thermal ellipsoids and lattice water are omitted for clarity, symmetry codes: i $-x + 1, -y + 1, -z + 1$; ii $x, y, z + 1$ (b) View of 2D polyhedron MnNO_5 and network sheets with chair modes. (c) View of 2D 4-c ($4^2.6^2$) topologic network

From the topological point of view, each Mn(II) center can be regarded as a 4-connecting tetrahedral node, while btca^{4-} and pbtrz ligands serve as linear linkers. As a result, the whole framework of **3** is reduced to a 2D 4-connected ($4^4.6^2$)-net layer (Fig. 3c), which is further extended by strong $\text{N-H}\cdots\text{O}$ and $\text{O-H}\cdots\text{O}$ hydrogen bonds to form a 3D supramolecular architecture.

Crystal Structure of $[\text{Mn}(\text{pbtrz})]_n \cdot n\text{OAc} \cdot n\text{OH}$ (**4**). Compound **4** crystallizes in the cubic space group $Ia\bar{3}d$, which is assembled into a 3D diamond shaped network with 1D channels. The asymmetric unit of **4** has one crystallographic independent Mn(II) cation, a half neutral pbtrz ligand, one OH^- and one CH_3COO^- (Fig. 4a). By contrast with **1**, **2** and **3**, each Mn(II) is four-coordinated with the donor set MnN_4 by two individual pbtrz ligands with $\mu\text{-N1,N4-trz}$ *cis*-binding mode. The difference attributes to 1,3-bis(1,2,4-triazol-1-yl)-propane in which flexible $-(\text{CH}_2)_3-$ spacers allow the triazolyl group to bend and rotate freely, then form the coordination geometries of metal cations [51, 52]. The distortion angles ($105.8(3)$ – $112.6(3)^\circ$) around the Mn(II) center indicate that the central Mn(II) cation lies in distorted tetrahedral geometry. The Mn–N (2.028(5), 2.039(5) Å) bond lengths are comparable to those of reported Mn(II) compounds [24, 53].

Each pbtrz ligand links three Mn(II) cations and each Mn(II) cation connects three pbtrz ligands. As a result, the cubic networks are formed with two kinds of closed channels, cross-sectional area about 5.92×14.3 and $7.2 \times 13.6 \text{ \AA}^2$ respectively (ignoring hydrogen atoms) (Fig. 4b). However, these channels are occupied with disordered OH^- and CH_3COO^- which act as counter anions to balance the charges (Fig. 4c). PLATON calculations [39] after removal of the disordered anions show that the potential anion exchange volume of **4** is estimated to 3068.3 \AA^3 , which constitutes approximately 49.2% of the unit cell volume. Due to the presence of $\bar{3}$ crystallographic symmetry, the packing of **4** along the crystallographic [111] axis created windmill-like cavity is shown in Fig. 4d. Topologically, by depicting Mn(II) cations as 4-connectors nodes, pbtrz ligands as linear linkers, the structure can be described as a 3D 4-connected $(4^2.6^2.8^2)$ network (Fig. 4e).

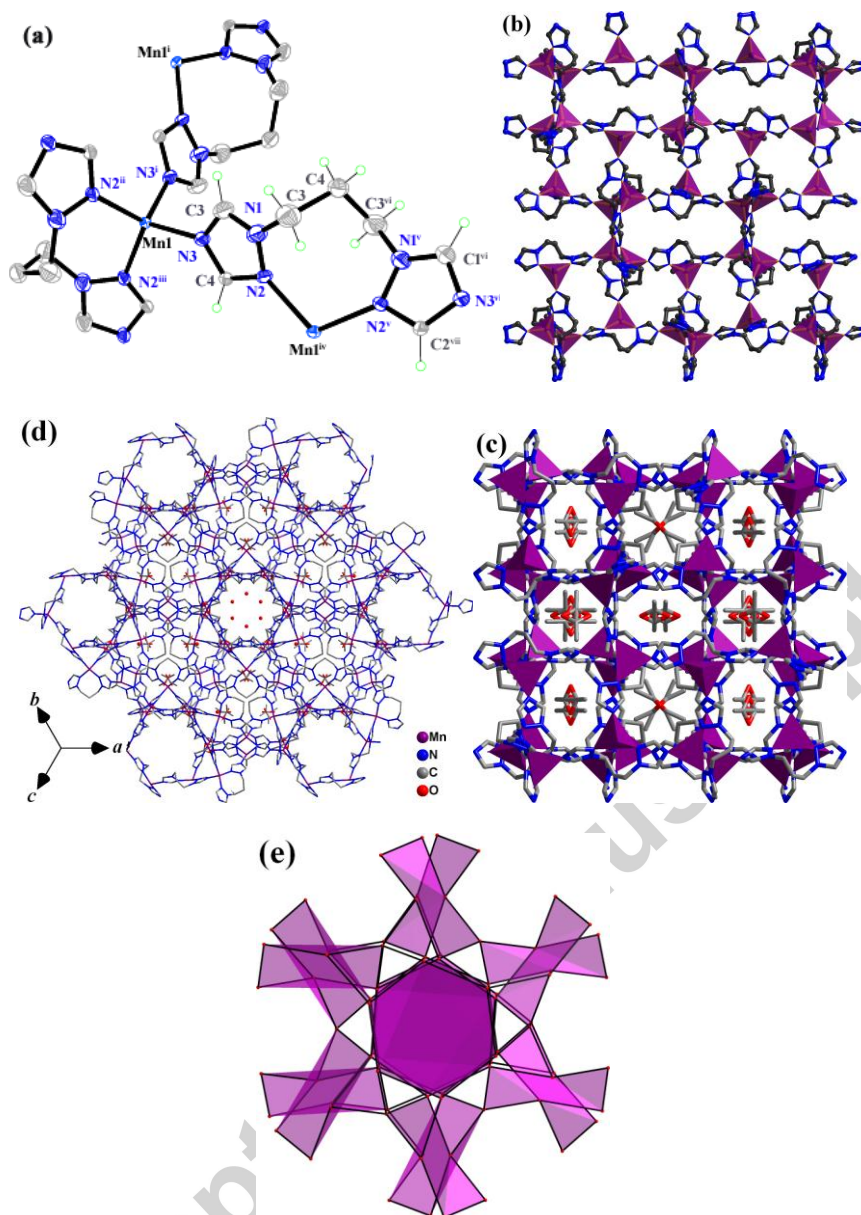


Fig. 4. (a) Coordination environments of Mn(II) in **4** with 15 % thermal ellipsoids. Part of H atoms and non-coordinated OH⁻ and CH₃COO⁻ are omitted for clarity. Symmetry codes: i $1/4 - x, -1/4 + z, 1/4 + y$; ii $-1/2 + z, +x, 1/2 - y$; iii $3/4 - z, 1/4 - y, 1/4 + x$; iv $-1/4 + z, 1/4 - y, 3/4 - x$; v $1/4 - y, 1/4 - x, 5/4 - z$; vi $1/4 - y, 1/4 + x, 3/4 - z$ (b) Unit cell packing diagrams with polyhedron MnN₄ viewed *a* axis. (c) Showing the closed channels with the counter anions and the OH⁻ anions adopt ball mode. (d) The illustration of 3D supermolecular frameworks of **4** is shown with windmill-like channel along the crystallographic [111] direction. (e) Schematic representation of the 4-c (4².6².8²) network.

3.4. PXRD and thermal analysis

PXRD patterns were obtained to check the purity of compounds **1–4** (Fig. S2). All the peaks displayed in the experimental patterns are similar to those in the simulated patterns generated from single-crystal diffraction data, demonstrating single phases.

TG analyses were performed on crystalline samples of compounds **1–4** to study their thermal stability (Fig. S3). TG curve of **1** shows a weight-loss of 10.7% (calcd: 11.2%) from 405 to 486 K corresponding to the release of two coordinated water molecules. Compound **1** begins to collapse at 895 K. Compound **2** exhibits a continuous two-step weight-loss stage from 453 K to 718 K corresponding to the collapse of the framework. Compound **3** displays a two-step weight-loss process. The first one is located on 393 K to 420 K due to the loss of two disordered lattice water molecules (calcd. 5.4%, found 5.6%). Once the temperature is higher than 643 K, the layered framework of **3** is broken, accompanying the decomposition of the compound. For **4**, a weight-loss of 7.1% in 298–661 K range is consistent with the removal the counter anions OH^- and CH_3COO^- as the relevant H_2O and CO_2 molecules (calcd. 7.1%). The 3D framework begins to collapse above 661 K.

3.5. Magnetic properties

Variable-temperature magnetic susceptibilities of **1–4** were measured in the range of 1.8–300 K under 1000 *Oe* and plots as $\chi_m T$, χ_m and χ_m^{-1} vs. T of **1–4** are shown in Figs. 5–8 Because of the various distinctions of topologies, their magnetic properties are very different.

[Mn(Hmctrz)₂(H₂O)₂] (**1**). As shown in Fig. 5, the $\chi_m T$ value of **1** is 4.91 cm³·K·mol⁻¹ at 300 K, corresponding to the expected one Mn(II) cation for an isolated $S = 5/2$ (4.38 cm³·K·mol⁻¹). Upon cooling, the $\chi_m T$ product of **1** steadily decreases from 300 to 20 K and then abruptly down to 3.33 cm³·K·mol⁻¹ at 1.8 K. The behaviour is consistent with dominant antiferro-magnetic interactions. The plot of χ_m^{-1} vs. T shows that **1** follows the Curie-Weiss law with $C = 4.94$ cm³·K·mol⁻¹ and $\theta = -0.58$ K, an indication of antiferromagnetic coupling between the Mn(II) units. Although compound **1** characterises chains of Mn(II) cations through the hydrogen bonds with Mn–OCO–Mn, the –OCO– bridge is very long (7.100 Å). Therefore, the coupling through this bridge is negligible. Accordingly, the decrease of the $\chi_M T$ below 10 K is most likely due to weak antiferromagnetic interactions between Mn(II) ions transmitted in the crystal lattice and/or the zero field splitting (ZFS) of the ⁶A_{1g} single-ion states.

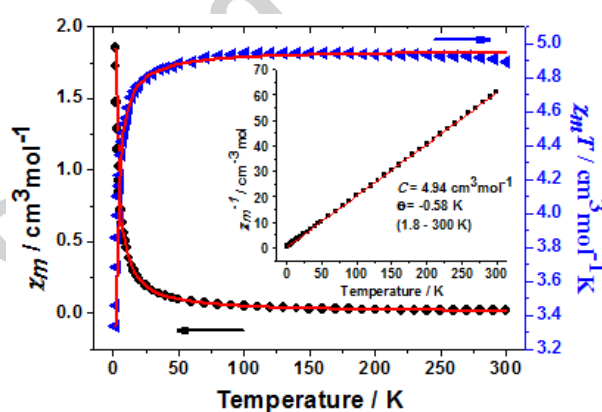


Fig. 5. Temperature dependence of χ_m , $\chi_m T$, and $1/\chi_m$ collected in an applied field of 1000 Oe for compound **1**. The red solid line represents the best fittings.

To explain magnetic properties of compound **1** composed of mononuclear Mn(II), we use Eq. (1) including ZFS effect within the $S = 5/2$ local ground states of the Mn(II) cations corrected by the factor predicted from the molecular field (Eq. 2) [54–56]:

$$\chi_{zfs} = \frac{Ng^2\beta^2}{4kT} \left[\frac{1 + 9\exp(2D/kT) + 25\exp(6D/kT)}{1 + \exp(2D/kT) + \exp(6D/kT)} \right] \quad (1)$$

$$\chi_m^{corr} = \frac{\chi_m}{1 - \frac{2zJ'}{N\beta^2g^2} \cdot \chi_m} \quad (2)$$

In the Eqs. (1) & (2), zJ' is the intermolecular exchange parameter; z is the number of nearest neighbour Mn(II) centers; D is the axial ZFS parameter for Mn(II), and the other symbols have their usual meaning. A least-squares fitting of the experimental data for **1** leads to $g = 2.085(2)$, $D = -0.129(1) \text{ cm}^{-1}$, $zJ' = -0.067(1) \text{ cm}^{-1}$ and $R = 2.24 \times 10^{-4}$. The criterion used in determination of the best fit is based on minimization of the sum of squares of the deviation: $R = \sum[(\chi_m T)_{\text{obsd}} - (\chi_m T)_{\text{calcd}}]^2 / [(\chi_m T)_{\text{obsd}}]^2$. This model reproduces very satisfactorily the magnetic properties of this compound in the whole temperature range (Fig. 5). Note that although this D value is within the normal range observed for isolated Mn(II) cations [57], it could include a very weak AF interaction. The negative D and θ values indicate AF exchange interactions between nearest-neighbour Mn cations in **1**.

$[\text{Mn}(\text{Hdctrz})(\text{H}_2\text{O})_2]_n$ (2). The $\chi_m T$ product of **2** is $4.70 \text{ cm}^3 \cdot \text{K} \cdot \text{mol}^{-1}$ at 300 K (Fig. 6), which is slightly higher than the expected value ($4.38 \text{ cm}^3 \cdot \text{K} \cdot \text{mol}^{-1}$) for one magnetically uncoupled Mn(II) cation with $S = 5/2$ and $g = 2.0$. The $\chi_m T$ value of **2** is a slightly decrease to $4.44 \text{ cm}^3 \cdot \text{K} \cdot \text{mol}^{-1}$ from 300 to 60 K. With a further decrease in temperature, the value of the $\chi_m T$ product decreases sharply, reaching a minimum value of $1.90 \text{ cm}^3 \cdot \text{K} \cdot \text{mol}^{-1}$ at 1.8 K. The magnetic susceptibility data follow the Curie–Weiss law above 2.0 K with a negative Weiss temperature $\theta = -4.59 \text{ K}$ and Curie constant $C = 4.77 \text{ cm}^3 \cdot \text{K} \cdot \text{mol}^{-1}$. The negative Weiss temperature suggests the presence of antiferromagnetic exchange interactions inside the Mn(II) dimer.

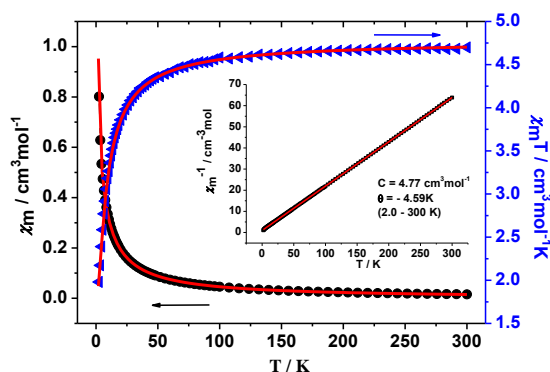


Fig. 6. Temperature dependence of χ_m , $\chi_m T$, and $1/\chi_m$ collected in an applied field of 1000 Oe

for **2**. The red solid lines represent the best fittings. Inset: temperature dependence of χ_m^{-1} .

To evaluate the exchange coupling, we have to identify the dominant interaction pathways in the metal–organic framework. As described in Fig. 2, though compound **2** is a 2D structure, the shortest Mn···Mn distance (7.069(1) Å) through the H₃dctrz bridge is longer than that through –OCO– bridge. So we suppose that magnetic interactions dominantly come from Mn–OCO–Mn chains, in which spin Heisenberg model for a one-dimensional chain or Fisher Model [58, 59] as Eqs. (3) & (4) is suitable for **2**.

$$\chi_{chain} = \frac{N_A g^2 \mu_B^2 S(S+1)}{3kT} \left[\frac{1+u}{1-u} \right] \quad (3)$$

where u is the Langevin function:

$$u = \coth \frac{JS(S+1)}{kT} - \frac{kT}{S(S+1)} \quad (4)$$

In order to take into account the intramolecular interactions in the 2D structure, the mean-field approximation zJ' is introduced shown in the Eq.(5) [59].

$$\chi_M = \frac{\chi_{chain}}{1 - \frac{2zJ' \times \chi_{chain}}{Ng^2 \beta^2}} \quad (5)$$

The best least-squares fitting of the magnetic susceptibility data presents $g = 2.0898$, $J = -0.354(4) \text{ cm}^{-1}$, $zJ' = -0.413(2) \text{ cm}^{-1}$, $R = 1.26 \times 10^{-4}$. The theoretical curves match the experimental data very well. The J and zJ' values confirm that the weak

antiferromagnetic couplings between intra- and interactions of Mn–OCO–Mn chains. However, it should be noted that the fitted values for J and zJ' are only qualitatively valid, because their comparability in magnitude does not meet the requirement of the molecular field approximation that zJ' should be much smaller than J [12]. All of these observations characterize the AF interactions in compound **2**.

$[\text{Mn}_2(\text{pbtrz})(\text{btca})]_n \cdot 4n\text{H}_2\text{O}$ (**3**). The experimental $\chi_m T$ value at 300 K is $9.65 \text{ cm}^3 \cdot \text{K} \cdot \text{mol}^{-1}$ (Fig. 7), which is a little smaller than that expected for a non-interacting pair antiferromagnetic interactions operating in **3**. The temperature dependence of the reciprocal susceptibilities χ_m^{-1} obeys the Curie–Weiss law above 2.0 K with a Weiss constant $\theta = -10.17 \text{ K}$, Curie constant $C = 10.0 \text{ cm}^3 \cdot \text{K} \cdot \text{mol}^{-1}$, indicating antiferromagnetic interactions in **3**.

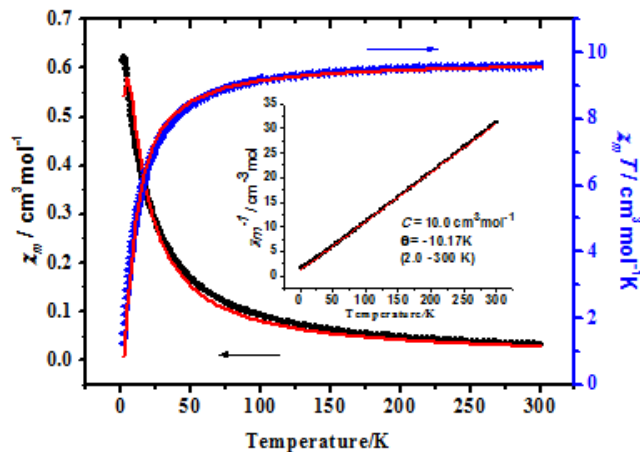


Fig. 7. Temperature dependence of χ_m , $\chi_m T$, and $1/\chi_m$ collected in an applied field of 1000 Oe for

3. The red solid line represents the best fittings. Inset: temperature dependence of χ_m^{-1} .

Structurally, the Mn1...Mn2 separation within a pair of corner-sharing octahedron is $3.698(1) \text{ \AA}$, which is smaller than those of $5.646(1)$ and $6.902(1) \text{ \AA}$ based on two bridges (pbtrz & btca⁴⁻) with zigzag projection on the bc plane. It could be presumed

that the main magnetic interactions come from Mn1 and Mn2 cations of corner-sharing octahedron, therefore, the magnetic interactions of **3** can be further simplify to a binuclear model with spin Hamiltonian $H = -2JS_1S_2$, in which the molecule field approximation can be introduced to evaluate the weak superexchange interaction transmitted by pbtrz and btca⁴⁻ bridges. The experimental molar magnetic susceptibilities of **3** can be quantitatively fitted by the following Eqs. (6) & (7).

$$\chi_{dimer} = \frac{2Ng^2\beta^2}{kT} \frac{A}{B} \quad (6)$$

$$A = 55 \exp 30x + 30 \exp 20x + 14 \exp 12x + 5 \exp 6x + \exp 2x$$

$$B = 11 \exp 30x + 9 \exp 20x + 7 \exp 12x + 5 \exp 6x + 3 \exp 2x + 1$$

$$x = J/kT$$

$$\chi_M = \frac{\chi_{dimer}}{1 - \frac{2zJ \times \chi_{dimer}}{Ng^2\beta^2}} \quad (7)$$

The best least-squares analysis of the magnetic susceptibilities data leads to $g = 2.011(6)$, $J = -0.696(6) \text{ cm}^{-1}$, $zJ' = 0.006(1) \text{ cm}^{-1}$, $R = 1.99 \times 10^{-4}$. The negative J value suggests weak antiferromagnetic interactions between the adjacent Mn(II) cations in **3**, which is also verified by the negative θ value.

$[\text{Mn}(\text{pbtrz})]_n \cdot n\text{OAc} \cdot n\text{OH}$ (4) As shown in Fig. 8, the observed $\chi_m T$ value for per Mn(II) unit of **4** is $34.22 \text{ cm}^3 \cdot \text{K} \cdot \text{mol}^{-1}$. It decreases almost linearly to $0.31 \text{ cm}^3 \cdot \text{K} \cdot \text{mol}^{-1}$ at 2.0 K when lowering the temperature. The behavior is clearly indicative of strong antiferromagnetic interactions between the Mn(II) centers. The result is similar to the previous magnetic study of 64 Fe^{3+} ions of $\{[\text{Fe}_8\text{O}_3(\text{tea})(\text{teaH})_3(\text{HCOO})_6]_8(\text{HCOO})_{12}\}(\text{ClO}_4)_{12} \cdot 3\text{CH}_3\text{OH} \cdot 36\text{H}_2\text{O}$ [60]. No satisfactory fit of the data is obtained now.

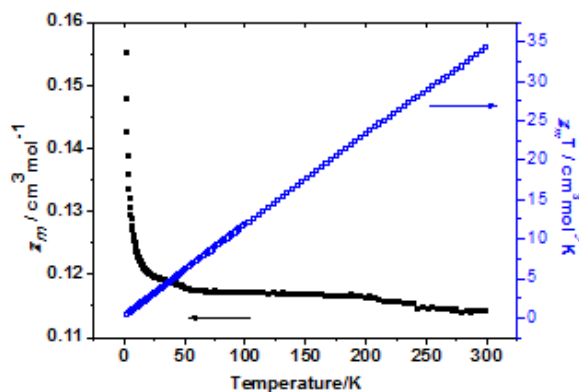


Fig. 8. Temperature dependence of χ_m and $\chi_m T$ collected in an applied field of 1000 Oe for **4**.

Apparently, interesting antiferromagnetic couplings with variable strengths are observed in the compounds **1–4**, which are significantly due to different superexchange interactions transmitted by the crystal lattice and/or the ZFS of the ${}^6A_{1g}$ single-ion states of **1** and the *syn-anti*-COO[−] of **2** as well as the mixed magnetic bridges of μ_1 -O and μ -pbtrz- μ -COO[−] of **3**. As we known, the bridging ligand can transfer magnetic exchange interactions through σ as well as π pathways, and a linker with only σ -bonding is a significantly weaker mediator [61]. For the present two compounds, the magnetic interactions are only mediated through σ pathway, which will result in weak antiferromagnetic interaction as observed.

4. Conclusion

In summary, four manganese magnetic samples based on 1,2,4-triazole and/or carboxylate bridges are designed and synthesized by control the temperature and/or the addition of co-ligands or nitrogenous bases. The templates as well as the pH value are key factors in determining the fundamental motifs and the dimensionality of the compounds based on H₃dctrz and the Mn(II) cation. It is found that the pbtrz can change the angles to meet the requirements of coordination and H₄btca has been successfully trapped in the neutral Mn(II) compound **3**. The antiferromagnetic

couplings with variable strength are observed in the nearest neighbours of **1–4**. In addition, compound **4** is a potential anion exchange material with the anion void volume 49.2% calculated by PLATON.

Supporting Information

X-ray crystallographic data for compounds **1–4** in CIF format (CCDC 1060382–1060385), selected bond lengths and bond angles, the figures of IR, PXRD and TG analysis are presented.

Acknowledgements

We acknowledge Zeng-Qiang Gao (BSRF) for the help of single-crystal X-ray diffraction data collection of **1** and **4** (line 3W1A), and acknowledge the financial support by the Natural Science Foundation of China (Grant Nos 21571118, 21201113 & 21671124). A portion of this work was performed on the Scientific Instrument Center of Shanxi University of China.

References

- [1] C. I. Yang, Z. Z. Zhang, S. B. Lin, *Coord. Chem. Rev.* 289–290 (2015) 289–314
- [2] W. J. Shi, L. Y. Du, H. Y. Yang, K. Zhang, L. Hou, Y. Y. Wang, *Inorg. Chem.* 56 (2017) 10090–10098

- [3] S. S. Feng, L. Xie, L. P. Lu, M. L. Zhu, F. Su. *J. Solid State Chem.* 258 (2018) 335–345
- [4] Y. Z. Zheng, Z. Zheng, X. M. Chen, *Coord. Chem. Rev.* 258 (2014)1–15
- [5] S.Y. Liu, J. P. Zhang, X. M. Chen, *Cryst. Growth Des.* 17 (2017) 1441–1449
- [6] P. Kar, M. G. B. Drew, C. J. Gómez-García, A. Ghosh, *Inorg. Chem.* 52 (2013) 1640–1649
- [7] T. G. Tziotzi, D. I. Tzimopoulos, T. Lis, R. Inglis and C. J. Milios, *Dalton Trans.* 44 (2015) 11696–11699
- [8] B. Gildea, M. M. Harris, L. C. Gavin, C. A. Murray, Y. Ortin, H. Mueller-Bunz, C. J. Harding, Y. Lan, A. K. Powell, G. G. Morgan, *Inorg. Chem.* 53 (2014) 6022–6033
- [9] T. G. Tziotzi, D. A. Kalofolias, D. I. Tzimopoulos, M. Siczek, T. Lis, R. Inglis, C. J. Milios, *Dalton Trans.* 44 (2015) 6082–6088
- [10] M. Sutradhar, L. M. D. R. S. Martins, M. F. C. Guedes da Silva, E. C. B. A. Alegria, C. M. Liu, A. J. L. Pombeiro, *Dalton Trans.* 43 (2014) 3966–3977
- [11] N. N. Mao, P. Hu, F. Yu, X. Chen, G. L. Zhuang, T. L. Zhang, B. Li, *CrystEngComm* 19 (2017) 4586–4594
- [12] S. Q. Bai, C. J. Fang, Z. He, E. Q. Gao, C. H. Yan, T. S. A. Hor, *Dalton Trans.* 41 (2012) 13379–13387

- [13] S. D. Han, J. P. Zhao, Y. Q. Chen, S. J. Liu, X. H. Miao, T. L. Hu, X. H. Bu, *Crys. Growth Des.* 14 (2014) 2–5
- [14] F. Su, L. P. Lu, S. S. Feng, M. L. Zhu, Z. Q. Gao and Y. H. Dong, *Dalton Trans.* 44 (2015) 7213–7222
- [15] Y. Yang, P. Du, Y. Y. Liu and J. F. Ma, *Cryst. Growth Des.* 13 (2013) 4781–4795
- [16] X. Y. Zhang, Z. Y. Liu, Z. Y. Liu, E. C. Yang, X. J. Zhao, *Z. Anorg. Allg. Chem.* 639 (2013) 974–981
- [17] J. Z. YAN, L. P. Lu, F. Su, M. L. Zhu, *Chinese J. Struct. Chem.* 34 (2015) 3401–3407
- [18] W. Ouellette, A. V. Prosvirin, J. Valeich, K. R. Dunbar, J. Zubieta, *Inorg. Chem.* 46 (2007) 9067–9082
- [19] Q. Ma, M. L. Zhu, L. P. Lu, S. S. Feng, J. Z. Yan, *Inorg. Chim. Acta* 370 (2011) 102–107
- [20] A. A. Dippold, T. M. Klapoetke, *J. Am. Chem. Soc.* 135 (2013) 9931–9938
- [21] W. Ouellette, S. Jones, J. Zubieta, *CrystEngComm* 13 (2011) 4457–4485
- [22] E. C. Yang, Z. Y. Liu, Y. L. Li, J. Y. Wang, X. J. Zhao, *Dalton Trans.* 40 (2011) 8513–8516

- [23] G. Ye, K. Y. Zou, Y. Yang, J. J. Wang, X. F. Gou, Z. X. Li, *J. Solid State Chem.* 225 (2015) 31–40
- [24] E. C. Yang, X. Y. Zhang, X. G. Wang, Z. Y. Liu, X. J. Zhao, *Polyhedron* 53 (2013) 208–214
- [25] L. H. Jia, A. C. Liu, B. W. Wang, Z. M. Wang, S. Gao, *Polyhedron* 30 (2011) 3112–3115
- [26] R. K. Mudsainiyan, A. Kaur Jassal, S.K. Chawla, *J. Solid State Chem.* 225 (2015) 249–255
- [27] A. N. Gusev, I. Nemeč, R. Herchel, E. Bayjyyev, G. A. Nyshchimenko, G. G. Alexandrov, I. L. Eremenko, Z. Travnicek, M. Hasegawa and W. Linert, *Dalton Trans.* 43 (2014) 7153–7165
- [28] L. Cheng, W. X. Zhang, B. H. Ye, J. B. Lin, X. M. Chen, *Inorg. Chem.* 46 (2007) 1135–1143
- [29] E. C. Yang, Z. Y. Liu, C. H. Zhang, Y. L. Yang, X. J. Zhao, *Dalton Trans.* 42 (2013) 1581–1590
- [30] Q. Ma, M. L. Zhu, L. P. Lu, S. S. Feng, T. W. Wang, *Dalton Trans.* 39 (2010) 5877–5884
- [31] J. P. Zhang, Y. Y. Lin, X. C. Huang and X. M. Chen, *Dalton Trans.* (2005) 3681–3685

- [32] G. M. Zhuang, X. B. Li, E. Q. Gao, *Inorg. Chem. Commun.* 47 (2014) 134–137
- [33] B. Xia, K. Wang, Q. L. Wang, Y. Ma, Y. Z. Tong, D. Z. Liao, *CrystEngComm* 19 (2017) 811–816
- [34] H. Liu, J. Tian, Y. Kou, J. Zhang, L. Feng, D. Li, W. Gu, X. Liu, D. Liao, P. Cheng, J. Ribas, S. Yan, *Dalton Trans.* (2009) 10511–10517
- [35] J. P. Costes, F. Dahan, B. Donnadiou, M. J. R. Douton, M. I. F. Garcia, A. Bousseksou and J. P. Tuchagues, *Inorg. Chem.* 43 (2004) 2736–2744
- [36] S. Baitalik, B. Dutta and K. Nag, *Polyhedron* 23 (2004) 913–919
- [37] Z. Otwinowski, W. Minor, *Methods in Enzymol.* 276 (1997) 307–326
- [38] SMART, SAINT and SADABS; Bruker AXS Inc., Madison, Wisconsin, USA, (1998)
- [39] G. Sheldrick, *Acta Crystallogr. A* 71 (2015) 3–8
- [40] G. Z. Liu, X. D. Li, X. L. Li, L. Y. Wang, *CrystEngComm* 15 (2013) 2428–2437
- [41] P. Majumdar, A. Pati, M. Patra, R. K. Behera and A. K. Behera, *Chem. Rev.* 114 (2014) 2942–2977
- [42] Y. Y. Liu, *Acta Crystallogr. E* 63 (2007) m1605
- [43] X. Q. Liang, D. P. Li, X. H. Zhou, Y. Sui, Y. Z. Li, J. L. Zuo, X. Z. You, *Cryst. Growth Des.* 9 (2009) 4872–4883

- [44] M. L. Han, X. H. Chang, X. Feng, L. F. Ma, L. Y. Wang, *CrystEngComm* 16 (2014) 1687–1695
- [45] X. Wang, D. Zhao, A. Tian, J. Ying, *CrystEngComm* 15 (2013) 4516–4526
- [46] K. Nakamoto, *Infrared and Raman Spectra of Inorganic and Coordination Compounds*. New York: Wiley, (1978)
- [47] J. Y. Liu, Q. Wang, L. J. Zhang, B. Yuan, Y. Y. Xu, X. Zhang, C. Y. Zhao, D. Wang, Y. Yuan, Y. Wang, B. Ding, X. J. Zhao, M. M. Yue, *Inorg. Chem.* 53 (2014) 5972–5985
- [48] S. Q. Sun, B. Zhang, P. J. Wu, D. B. Zhu, *J. Chem. Soc., Dalton Trans.* 2 (1997) 277–281
- [49] Y. Y. Liu, *J. Coord. Chem.* 60 (2007) 2597–2605
- [50] O. M. Yaghi, G. M. Li, T. L. Groy, *J. Chem. Soc., Dalton Trans.* (1995) 727–732
- [51] C. J. Zhang, H. J. Pang, Q. Tang, H. Y. Wang, Y. G. Chen, *Dalton Trans.* 39 (2010) 7993–7999
- [52] B. Liu, Z. T. Yu, J. Yang, W. Hua, Y. Y. Liu, J. F. Ma, *Inorg. Chem.* 50 (2011) 8967–8972
- [53] J. Z. Fan, C. C. Du, D. Z. Wang, *Polyhedron* 117 (2016) 487–495

- [54] P. Kar, M. G. B. Drew, C. J. Gomez-Garcia, A. Ghosh, *Polyhedron* 50 (2013) 229–239
- [55] S. Konar, S. C. Manna, E. Zangrando, T. Mallah, J. Ribas, N. R. Chaudhuri, *Eur. J. Inorg. Chem.* 43 (2004) 4202–4208
- [56] J. S. Smart, *Effective Field Theories of Magnetism*, W. B. Saunders Comp., Philadelphia, London, (1996)
- [57] R. Boca, *Coord. Chem. Rev.* 248 (2004) 757–815
- [58] O. Kahn, *Molecular Magnetism*, VCH, New York, (1993) 251–286
- [59] M. E. Fisher, *Am. J. Phys.* 32 (1964) 343–346
- [60] T. Liu, Y. J. Zhang, Z. M. Wang, S. Gao, *J. Am. Chem. Soc.*, 130 (2008) 10500–10501
- [61] J. R. Galán-Mascarós and K. R. Dunbar, *Angew. Chem. Int. Ed.*, 42 (2003) 2289–2293

Highlights

1. Four manganese (II) compounds are synthesized and fully characterized.
2. The complexes are built by 1,2,4-triazole and carboxylate bifunctional-group.
3. Complexes **1-3** show antiferromagnetic coupling fitted by different models.
4. Complex **4** is a potential anion exchange porous material.

Graphical Abstract

Four new Mn^{II} complexes based on 1,2,4-triazole and carboxylate bifunctional-group show structural diversities and antiferromagnetic couplings.

